



TECHNICAL REPORT 2016 Rev. 1  
April 2013

## **Convergence of the Quasi-static Antenna Design Algorithm**

T. O. Jones III

Approved for public release.

SSC Pacific  
San Diego, CA 92152-5001



TECHNICAL REPORT 2016 Rev. 1  
April 2013

# Convergence of the Quasi-static Antenna Design Algorithm

T. O. Jones III

Approved for public release.



SSC Pacific  
San Diego, CA 92152-5001

**SSC Pacific**  
**San Diego, California 92152-5001**

---

---

**J.J. Beel, CAPT, USN**  
**Commanding Officer**

**C. A. Keeney**  
**Executive Director**

**ADMINISTRATIVE INFORMATION**

This report was prepared for the by the ISR/IO Department (Code 56), SPAWAR Systems Center Pacific, San Diego, CA.

Released by  
M. D. Osburn, Head  
Electromagnetics Technology  
Branch

Under authority of  
J. McGee, Head  
SoS & Platform Design  
Division

This is a work of the United States Government and therefore is not copyrighted. This work may be copied and disseminated without restriction.

MATLAB<sup>®</sup> is a registered trademark of The Math Works.

## EXECUTIVE SUMMARY

The quasi-static antenna design algorithm is a scientific approach to designing electrically small antennas. Electrically small antennas are small compared to wavelength. The radiation resistance is computed from the electrostatic dipole potential. The capacitance is computed from the electrostatic potential on the enclosed sphere. The  $Q$  is calculated from the radiation resistance and capacitance. The general thick-disk-cap monopole, enclosed by a sphere, is modeled with electrostatic multipole basis functions on the disk. A sequence of solutions converges in shape and  $Q$ .

Computer Simulation Technology (CST) Microwave Studio is used to compute the impedance of the thick-disk-cap monopole. The impedance is numerically fit to the dipole and octupole eigenmode equivalent circuit. The antenna eigenmodes are analogous to radio frequency (RF) cavity eigenmodes. The radiation resistance is computed from the dipole eigenmode. The DC capacitance is accurately computed. The current sharing between the dipole and octupole eigenmodes slightly decreases the radiation resistance and slightly increases the antenna  $Q$ . The quasi-static antenna design algorithm is a good approximation of the exact solution.

The figure of merit is the  $Q$ -factor ratio, the ratio of the  $Q$  to  $Q_{\text{Chu}}$ , L. J. Chu's [1] theoretical limit for an antenna enclosed by a sphere. The thick-disk-cap monopole has the absolute minimum  $Q$ -factor ratio of 1.825. The spherical-cap monopole has a slightly lower  $Q$ -factor ratio of 1.75. At the resonance, the thick-disk-cap monopole's  $Q$  is 22.5. This is much smaller than the spherical-cap monopole's  $Q$  of 46.1. Above the resonant frequency, the thick-disk-cap monopole is a superior design.



# CONTENTS

EXECUTIVE SUMMARY .....	iii
1. INTRODUCTION .....	1
2. CAPACITANCE FOR THE OBLATE SPHEROIDAL ANTENNA .....	5
3. GENERAL CALCULATION OF RADIATION RESISTANCE .....	9
4. GENERAL OBLATE SPHEROIDAL ANTENNA .....	11
5. SECTION CST MODEL OF OBLATE SPHERICAL ANTENNA.....	13
6. CST MODEL OF A SPHERICAL-CAP MONOPOLE .....	23
7. CONCLUSION.....	29
8. REFERENCES .....	31

## Figures

1. First four top-load radial multipole basis functions.....	7
2. A sequence of antenna designs with one to five load multipoles.....	11
3. The antenna shape near the enclosing surface.....	12
4. Electric field calculated as a function of distance from the antenna top .....	12
5. The three-dimensional OSA surface with a 45° slice removed.....	14
6. The equivalent circuit for the first and second eigenmode approximation .....	14
7. CST data and two-eigenmode equivalent circuit model.....	17
8. Difference between the CST data and the two-eigenmode model for $ \rho  < 0.9$ .....	18
9. The $\omega^2$ and $\omega^4$ contribution to resistance.....	19
10. Q for the minimum Q OSA design .....	20
11. Q-factor ratio for the minimum Q OSA design .....	21
12. CST impedance and two-eigenmode model.....	24
13. Difference between the CST data and the two-eigenmode model .....	25
14. The $\omega^2$ and $\omega^4$ components of resistance .....	26
15. Q for spherical-cap monopole .....	27
16. Q-factor ratio for spherical-cap monopole.....	28

## Tables

1. Least square best fit to Stuart's eigenmode impedance circuit model .....	15
2. Spherical-cap monopole impedance is fit to a two-eigenmode model.....	23



# 1. INTRODUCTION

Electrically small antennas are common to portable electronics devices, personal digital assistants (PDAs), cell phones, etc. These antennas are small compared to wavelength, i.e., electrically small antennas. Designing electrically small antennas is an art; they normally have a low radiation resistance, a large reactance, and a narrow bandwidth. Electrically small antennas are used when reducing the antenna size is a critical design goal. Additional matching components are required to eliminate the reactance and increase the resistance. The objective is to develop a scientific method for designing electrically small antennas. The radiation resistance and capacitance are optimized to give the minimum  $Q$  antenna.

L. J. Chu [1] derived a lower limit for the  $Q$  of electrically small antennas. Chu's  $Q$  calculation is based on the radiated energy and the stored energy outside a sphere enclosing the antenna; the energy inside the sphere is assumed to be zero. H. L. Thal [2] refined this limit by assuming the antenna current is limited to the surface of the enclosing surface. The folded spherical helix design by S. R. Best [3] meets Thal's limit. M. Gustafsson, C. Sohl, and G. Kristensson [4] derived a  $Q$  limit based on the optical theorem. A. D. Yaghjian and H. R. Stuart [5] derived a more restrictive limit on  $Q$ .

The energy inside the sphere limits the antenna performance. The thin-disk-cap monopole is a leaky capacitor with a large amount of stored energy inside the sphere. The electric field under the disk is larger than the field above the disk. The quasi-static antenna design algorithm [6, 7] analytically computed a thick-disk-cap monopole. The thick-disk cap reduces the stored energy and  $Q$  by filling some of the spherical volume with conductor. The electric field under the top load is still larger than the field above the top load. This paper shows how to reduce the electric field under the top load and increase the radiation resistance of the antenna [8]. The antenna shape shifts to eliminate the gap (and the energy) between the top of the antenna and the enclosing sphere. The stored energy inside the enclosing sphere is limited to the region between the antenna and the ground.

Electrically small antennas have electric fields much larger than the magnetic fields below the antenna resonance. The Asymptotic Conical Dipole (ACD) [9, 10, and 11] was the first antenna designed with quasi-static methods. In electrostatics, a perfect conductor is the same as an equipotential surface. A line of constant charge on the  $z$ -axis, with an image, will generate the ACD antenna design. Each ACD antenna has a different height. The quasi-static antenna design algorithm [7] fixes the antenna height to a constant  $a$  and the length of the line charge  $\kappa a$  is varied; the antenna fits within an enclosing sphere with a radius  $a$ . The parameter  $\kappa$  is a dimensionless. The  $Q$  is calculated from

$$Q = \frac{1}{\omega C R_{Rad}}, \quad (1)$$

where  $R_{Rad}$  is radiation resistance,  $C$  is capacitance, and  $\omega$  is angular frequency. The quantities  $R_{Rad}$  and  $C$  are functions of  $\kappa$ . The radiation resistance is calculated from the effective height. The capacitance is calculated from the charge on the antenna arm and the maximum potential on the spherical enclosing surface.

The above equation for  $Q$  is valid below resonance and it gives only the first term in Chu's equation:

$$Q > \frac{1}{(ka)^3} + \frac{1}{ka}, \quad (2)$$

where  $k = 2\pi / \lambda$  and  $a$  is the radius of the enclosing sphere. The ACD design is extended by adding a disk-shaped charge distribution as a load on the line charge [7]. A conducting disk in free space is used as the charge distribution. This disk charge distribution is symmetric. The electric fields between the disks and image will be larger than the electric fields above the disk. There is no requirement for the disk charge distribution to be symmetric. Adding a dipole moment moves the charge from the bottom of the disk to the top of the disk. This reduces the electric field between the disks. A series of multipole charge distributions can be added to the disk to model the general charge distribution on the disk.

Sections 2 and 3 are not needed to understand the results given in Sections 4 and 5. Section 2 shows how the potential and top load capacitance is computed from electrostatic solutions in oblate spheroidal coordinates. Each solution represents a unique multipole moment with an unique potential. Only the rotationally symmetric top-load multipole modes will be used in this model. The  $n^{\text{th}}$  multipole moment falls off as  $\frac{1}{r^{n+1}}$  in the far field. The potential for the dipole multipole term and higher odd multipole moments add in the far field. The monopole and higher even multipole moments cancel in the far fields. All of the multipoles make a unique and diminishing contribution to the near fields. In section 3, the effective height is calculated. The effective height calculation with dipole moment top load is non-trivial. The effective height cannot be calculated with the conventional formula [8]. The effective height is calculated indirectly from the potential on the enclosing sphere. The perfect conductor boundary condition,  $E_{\parallel} = 0$ , requires the charge distribution to be enclosed by the antenna surface. Only a subset of the charge distributions satisfies this boundary condition. The multipole moments have negative potentials, which can cause the equipotential surface to terminate on the disk or feed wire. This requires an addition step in the solution process; the equipotential surface is sampled to verify that the charge is enclosed by the equipotential surface. The final solution must be verified with a detailed calculation of the antenna shape. In Section 4, a sequence of multipole basis functions is used to design minimum Q antennas. The antenna designs appear to converge in both shape and  $Q$ . The final antenna design fills the top of the sphere; the area under the antenna is the only region with electric fields that contributes to stored energy inside the enclosing sphere. The electric field on the surface of the antenna is plotted. The electric field under the antenna is reduced by adding the dipole moment. The final antenna has an almost horizontal lower surface.

In Section 5, Computer Simulation Technology (CST) Microwave Studio is used to calculate the impedance and  $Q$  for a 1-m high antenna with a 1-cm-diameter feed line. The impedance is calculated with a sequence of energy-based adaptive iterations. L. J. Chu [1], H. D. Foltz, J. S. McLean, and L. Bodner [12], and H. Stuart [13] used a series,  $L$ ,  $C$ , with a resistor,  $R_0$ , parallel to the inductor to model both the reactance and  $\omega^2$  dependence radiation resistance. The model represents the dipole eigenmode. The least squares fit to the CST impedance is a good fit to the reactance. For the resistance, the two curves cross at only on point; at other points the percentage error is large. The radiation resistance has an  $\omega^2$  and  $\omega^4$  frequency-dependent terms; the coefficients are calculated with a least square fit. The  $\omega^2$  contribution gives the same effective height as the quasi-static antenna design algorithm. The  $\omega^4$  frequency-dependent term is the source

of the error in the circuit model.

The next eigenmode, the octopole, is a circuit connected in parallel with the dipole eigenmode model [13]. The octopole (and higher) equivalent circuits reduce to a capacitor at low frequencies. The radiation resistance for the octopole eigenmode is not included in the simple equivalent circuit. This capacitance combined with dipole eigenmode circuit gives an antiresonance. The dipole and octopole eigenmode currents interfere with each other to create a high impedance at antiresonance. A least square iteration method was used to calculate the circuit elements. The improved fit to the radiation resistance data is attributed to a  $\omega^4$  frequency-dependent term introduced by the parallel capacitance. An analysis of the circuit impedance shows that current sharing between the eigenmodes introduces a small error in the quasi-static antenna design algorithm. The  $Q$  and resistance are modified by current sharing factor. The DC capacitance is accurate. The extra capacitance introduced by the feed line is estimated.

In Section 6, CST is also used to calculate the impedance of the spherical-cap monopole. The same feed wire was used for the 1-m spherical-cap monopole. The data is fit to the same dipole eigenmode with a capacitor approximation of higher eigenmodes. The capacitance of the top-load is larger than the above design. The effective height is smaller. The Q-factor ratio is about the same as the result obtained by A. R. Lopez [14]. Electrostatic data is not available to compare to the circuit results.

Section 7 is the conclusion. The quasi-static antenna design algorithm gives a solution very close to the spherical-cap monopole (the top-loaded monopole design with the lowest  $Q$ ). The algorithm does not model all possible antenna shapes. The algorithm only considers antenna shapes that enclose the source charge on the disk. A thick-spherical-cap monopole could have a lower  $Q$ . The quasi-static antenna design algorithm produces a very good antenna design with modest effort. Other designs can be computed with a significantly higher radiation resistance and a slightly larger  $Q$ . The algorithm can be adapted to other enclosing surfaces.



## 2. CAPACITANCE FOR THE OBLATE SPHEROIDAL ANTENNA

The detailed discussion of the algorithm is given in Reference 7. This discussion is the general case. The capacitance of the general thick-disk cap is calculated from the potential on enclosing surface ( $q = CV$ ). The potential is calculated from an analytic solution to the electrostatic equations. The top of the feed line has a height  $\kappa a$  and  $(1-\tau)q$  charge; the potential [15, 16] is

$$\Phi^{ACD}(\rho, z) = \frac{(1-\tau)q}{4\pi\epsilon_0\kappa a} \ln\left(\frac{(1+\delta_m)(1-\delta_i)}{(1-\delta_m)(1+\delta_i)}\right), \quad (3)$$

where  $\delta_m = \frac{\kappa a}{R_f + R_i}$  is for the monopole,  $\delta_i = \frac{\kappa a}{R_f + R_b}$  is for the image monopole,  $R_i = \sqrt{(z - \kappa a)^2 + \rho^2}$  is the distance from  $\rho, z$  to the top of the monopole,  $R_f = \sqrt{z^2 + \rho^2}$  is the distance from  $\rho, z$  to the feed point, and  $R_b = \sqrt{(z + \kappa a)^2 + \rho^2}$  is the distance from  $\rho, z$  to the bottom of the image monopole. The parameter  $\tau$  is the fraction of the total charge  $q$  on the antenna top load. The superscript indicates an ACD stem. The parameter  $\kappa$  is dimensionless,  $0 < \kappa < 1$ . The stem radius is not constant; it tapers to a zero as the feed point is approached

The disk also has the height  $\kappa a$ , a disk radius of  $\alpha a$ , and a net charge  $\pi q$  where the parameter  $\alpha$  is dimensionless and has the range of values  $0 < \alpha < \sqrt{1 - \kappa^2}$ . G. Arfken [17, pp. 599-601 and 596] gives the general solution to potential on the disk,  $\nabla^2 \Phi(u, v, \phi) = 0$ . The potential on the disk is a linear combination of multipole moments,  $K_n^m(u) P_n^m(\cos v) e^{im\phi}$ , where  $v$  and  $u$  are defined by the oblate spheroidal coordinate system:

$$z = \alpha a \sinh(u) \cos(v), \quad (4)$$

$$x = \alpha a \cosh(u) \sin(v) \cos(\phi), \quad (5)$$

$$y = \alpha a \cosh(u) \sin(v) \sin(\phi), \quad (6)$$

where  $\alpha a$  is the disk radius. The antenna's design with coordinate system is called an oblate spheroidal antenna (OSA). The antenna problem will be simplified by assuming rotational symmetry where  $\rho = \alpha a \cosh(u) \cos(v)$ :

$$\Phi(u, v, \phi) = \sum_{n=0}^{\infty} \sum_{m=0}^{m=n} \frac{b_{nm}}{\alpha^n} K_n^m(u) P_n^m(\cos v) e^{im\phi}. \quad (7)$$

The rotational symmetry in  $\phi$  requires  $b_{mn} = 0$  for  $m > 0$  and the associated Legendre Polynomials reduce to Legendre Polynomials,  $P_n^0(\cos \nu) = P_n(\cos \nu)$ . The  $1/\alpha^n$  is added for numerical convenience. The  $K_n(u)$  functions are as follows:

$$K_0(u) = \operatorname{arccot}(\sinh u), \quad (8)$$

$$K_1(u) = 1 - \sinh(u) \operatorname{arccot}(\sinh(u)), \quad (9)$$

$$K_2(u) = [(3 \sinh^2(u) + 1) \operatorname{arccot}(\sinh(u)) - 3 \sinh(u)]/2, \quad (10)$$

and

$$K_3(u) = -\left(\frac{5}{2} \sinh^3(u) + \frac{3}{2} \sinh(u)\right) \operatorname{arccot}(\sinh(u)) + \frac{5}{3} \left(\frac{3}{2} \sinh^2(u) + \frac{1}{2}\right) - \frac{1}{6}. \quad (11)$$

The general case is

$$K_n(\xi) = (-i^{n+1}) Q_n(i\xi), \quad (12)$$

where

$$Q_n(i\xi) = (-i) P_n(i\xi) \operatorname{arccot}(\xi) - \frac{(2n-1)}{n} P_{n-1}(i\xi) - \frac{(2n-5)}{3(n-1)} P_{n-3}(i\xi) - \dots \quad (13)$$

The function  $K_n$  at large distance is calculated by expanding  $a \cot(\sinh(u)) = a \tan(1/\sinh(u))$  in a power series of  $\frac{1}{\sinh(u)}$ . After simplifying, the leading term is

$$K_0 \approx \frac{1}{\sinh(u)} \quad \text{for } u \gg 2, \quad (14)$$

$$K_1 \approx \frac{2}{3} \frac{1}{\sinh^2(u)} \quad \text{for } u \gg 2, \quad (15)$$

$$K_2 \approx \frac{2}{15} \frac{1}{\sinh^3(u)} \quad \text{for } u \gg 2, \quad (16)$$

and

$$K_3 \approx \frac{2}{35} \frac{1}{\sinh^4(u)} \quad \text{for } u \gg 2 \quad (17)$$

since  $\alpha a \sinh(u) = z$ , the above equations reduce to  $\frac{\alpha a}{z}$ ,  $\frac{2}{3} \left(\frac{\alpha a}{z}\right)^2$ ,  $\frac{2}{15} \left(\frac{\alpha a}{z}\right)^3$ , and  $\frac{2}{35} \left(\frac{\alpha a}{z}\right)^4$ . This is the expected multipole expansion of the field on the z-axis. Figure 1 plots  $K_n$  as a function of  $\sinh(u)$ ; the plot shows the  $\frac{1}{z^{n+1}}$  dependence. The factor  $\frac{1}{\alpha^n}$  is included in Equation (7) to eliminate the  $\alpha^n$  dependence in the far field. The value of  $b_{00} = \frac{\tau q}{4\pi\epsilon_0 a}$  is calculated from the solution of the charged conducting disk in free space  $V(u) = \frac{\tau q}{4\pi\epsilon_0 \alpha a} \operatorname{arccot}(\sinh u)$ , where  $\tau q$  is the net charge on the disk. The only restriction placed on the values of  $b_{nm}$  is the charge distribution must be enclosed within an equipotential surface.

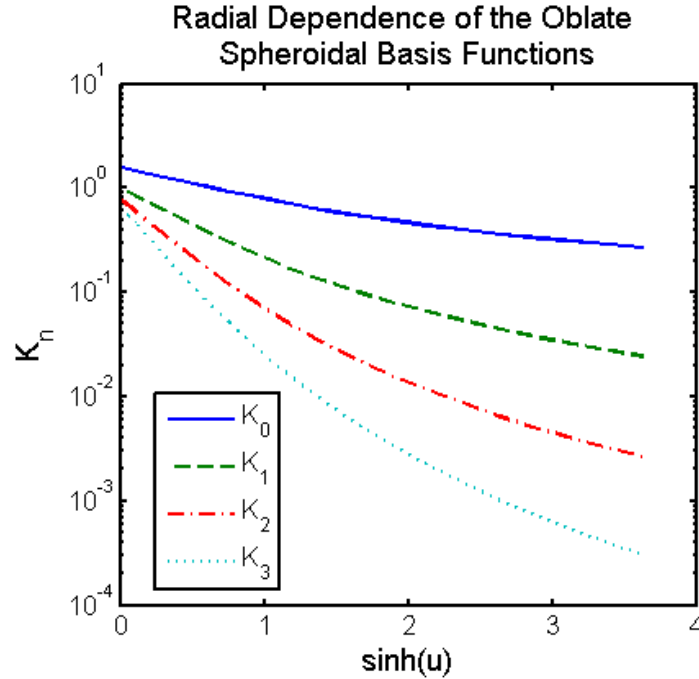


Figure 1. First four top-load radial multipole basis functions.

The combined potential is

$$\Phi(z, \rho) = \Phi^{ACD}(\rho, z) + \Phi^{TopDisk}(u_t, v_t) + \Phi^{BotDisk}(u_b, v_b), \quad (18)$$

where the variables  $u_t$ ,  $v_t$ , and  $u_b$ ,  $v_b$  are defined from

$$z - \kappa a = \alpha a \sinh(u_t) \cos(v_t), \quad (19)$$

$$\rho = \alpha a \cosh(u_t) \sin(v_t), \quad (20)$$

$$z + \kappa a = \alpha a \sinh(u_b) \cos(v_b), \quad (21)$$

$$\rho = \alpha a \cosh(u_b) \sin(v_b). \quad (22)$$

The capacitance is calculated from the maximum value of  $\Phi(z, \rho)$  on the sphere  $z = a \cos \theta$  and  $\rho = a \sin \theta$ :

$$\Phi_{Max} = \max(\Phi(a \cos \theta, a \sin \theta)) \text{ where } 0 \leq \theta \leq \pi/2 \quad (23)$$

and

$$C = \frac{q}{\Phi_{Max}}. \quad (24)$$

In the above coordinate systems,  $v_t = 0$  and  $v_b = 0$  are defined in the  $+z$  direction. The charge distribution that generates the term  $\Phi^{BotDisk}(u_b, v_b)$  is the mirror image of the charge distribution for  $\Phi^{TopDisk}(u_t, v_t)$ :

$$\Phi^{TopDisk}(u_t, v_t) = \sum_{n=0}^{\infty} \frac{b_n}{\alpha^n} K_n(u_t) P_n(\cos v_t) \quad (25)$$

and

$$\Phi^{BotDisk}(u_b, v_b) = - \sum_{n=0}^{\infty} (-1)^n \frac{b_n}{\alpha^n} K_n(u_b) P_n(\cos v_b). \quad (26)$$

The sign on  $\frac{b_n}{\alpha^n} K_n(u_b) P_n(\cos v_b)$  follows from  $P_n(\cos v_b)$ , being even or odd relative to  $v = \pi/2$ . The dipole term is the simplest example to understand:  $K_1(u_t) P_1(\cos v_t)$  has positive charge on the top of the disk and  $K_1(u_b) P_1(\cos v_b)$  has positive charge on the top of the image disk (top is  $+z$  direction for both disks). Both terms have a negative charge on the bottom of the disk and image disk. The combined terms

$$K_1(u_t) P_1(\cos v_t) + K_1(u_b) P_1(\cos v_b) \quad (27)$$

are odd about  $z = 0$ . For the case,  $b_1 > 0$ , the dipole moment of the antenna is increased and the electric field under the disk is decreased (with the other parameters unchanged). In the general case, when  $n$  is odd, the terms

$$K_n(u_t) P_n(\cos v_t) + K_n(u_b) P_n(\cos v_b) \text{ for odd } n \quad (28)$$

increases the  $n^{th}$  multipole moment. When  $n$  is even, the terms

$$K_n(u_t) P_n(\cos v_t) - K_n(u_b) P_n(\cos v_b) \text{ for even } n \quad (29)$$

subtract in the far field the first contributing far-field moment is the  $(n+1)^{th}$  multipole moment. Each term has a unique contribution to the electric field under the antenna.

The next step is to compute the radiation resistance.

### 3. GENERAL CALCULATION OF RADIATION RESISTANCE

The effective height for a rotationally symmetric charge distribution is

$$h_{Eff} = \frac{1}{q_{Net}} \int_{z=0}^{z=a} \int_{\rho=0}^{\rho=\sqrt{a^2-z^2}} zq(\rho, z) 2\pi\rho d\rho dz. \quad (30)$$

From a previous paper [6, 7], this simplifies to

$$h_{Eff} = \frac{\kappa a}{2} (1 - \tau) + \kappa a \tau. \quad (31)$$

The application of the above effective height calculation to the dipole term  $K_1(u)P_1(\cos \nu)$  is not obvious. The  $K_1(u)P_1(\cos \nu)$  term is discontinuous at  $u = 0$ . The function is odd about  $\nu = \pi/2$  or  $K_1(0)P_1(\cos \nu) = -K_1(0)P_1(\cos(\pi - \nu))$ . The dipole term would give zero for a thin disk with no net charge.

To derive the general case, the dipole moment used as the starting point is

$$\mathbf{p}_z = \int_{z=-a}^{z=a} \int_{\rho=0}^{\rho=\sqrt{a^2-z^2}} zq(\rho, z) 2\pi\rho d\rho dz. \quad (32)$$

The potential outside (and on) the sphere can be represented as a sum of spherical harmonics:

$$\Phi(r, \theta) = \sum_{n=1}^{\infty} \beta_{n0} \left(\frac{a}{r}\right)^{n+1} P_n(\cos \theta) \text{ for } r \geq a, \quad (33)$$

where  $r = \sqrt{z^2 + \rho^2}$  with all of the charge enclosed in a sphere of radius  $a$ . The dipole moment is computed from the potentials,

$$\mathbf{p}_z = \frac{3}{2} a^2 \int_{\theta=0}^{\theta=\pi} \Phi(a, \theta) P_1(\cos \theta) \sin \theta d\theta. \quad (34)$$

The two equations yield  $p_z = \beta_{10} a^2$ . The effective height is

$$h_{Eff} = \frac{1}{2q_{Net}} |\mathbf{p}_z|. \quad (35)$$



## 4. GENERAL OBLATE SPHEROIDAL ANTENNA

In the calculation for the thin-disk-cap monopole, the feed line is neglected. The capacitance calculation assumes all of the charge is on the top load disk. The MATLAB<sup>®</sup> calculation of the oblate spheroidal antenna assumes that 99% of the charge is on the top load and a token 1% of the charge is on the feed line:  $\tau = 0.99$  and  $(1-\tau)=0.01$ . The 1% charge on the feed line makes a ½% change on the radiation resistance and about a 1% change in the capacitance. The feed line radius tapers to zero at the feed point. As shown in Figure 2, the antenna designs with four and five multipoles are almost identical and Q-factor ratios have a 0.03% difference. The antenna design appears to converge in shape and Q-factor ratio.

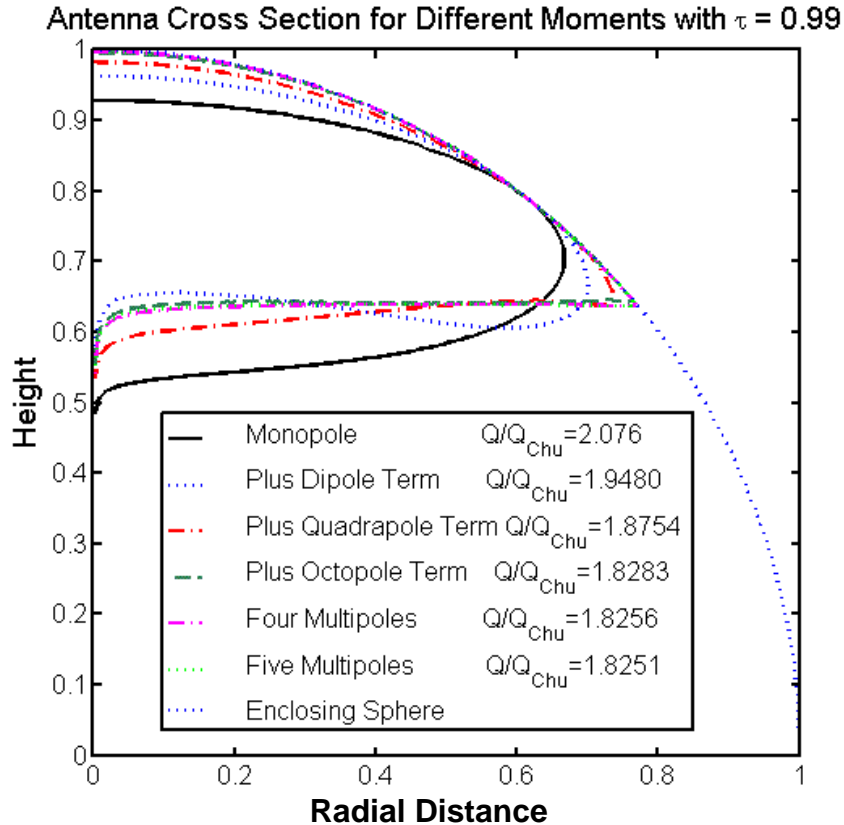


Figure 2. A sequence of antenna designs with one to five load multipoles.

Figure 3 shows a detailed plot of the antenna surface near the sphere. Spherical coordinates  $r = \sqrt{z^2 + \rho^2}$  are used for the vertical axis and  $\theta = \arcsin(\rho/r)$  is used for the horizontal axis. As basis functions are added to the antenna design, the shape approaches the surface of the enclosing sphere. Figure 3 shows that adding extra multipole moments has a diminishing impact on the Q-factor ratio. The multipole moments fall off as  $1/r^{n+1}$ ; they have diminishing impact on the electric field outside the sphere and under the antenna.

The electric field is calculated from the potential and is plotted in Figure 4. The vertical scale is electric field magnitude plotted as a function of distance along the surface measured from the top of the antenna,  $z = 1$  and  $\rho = 0$ . The electric field under the antenna is reduced by the dipole moment

term. The spike in the electric field is at the transition from almost spherical surface to the antenna underside. For the solution with five multipoles, this transition is very sharp. Figure 4 shows that the position of the spike moves to the right as multipoles are added. The added multipoles are increasing the surface area of the top of the antenna and the total charge on the top of the antenna.

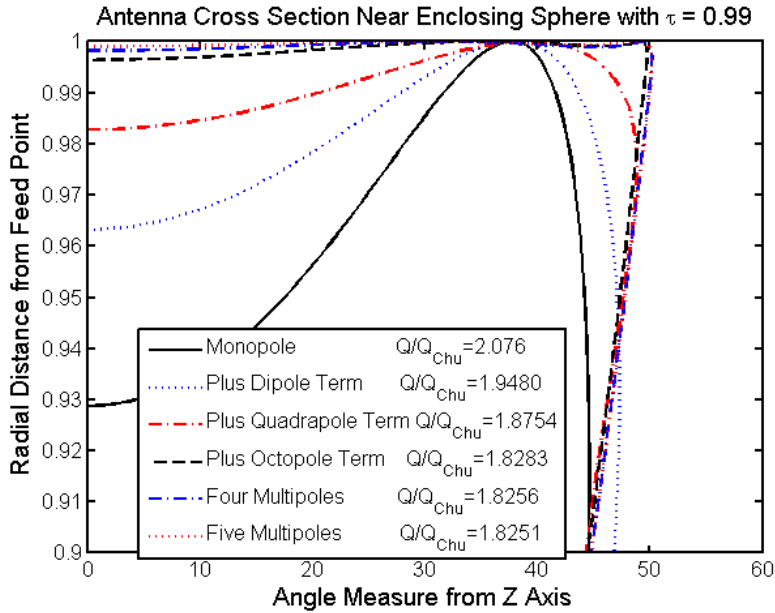


Figure 3. The antenna shape near the enclosing surface.

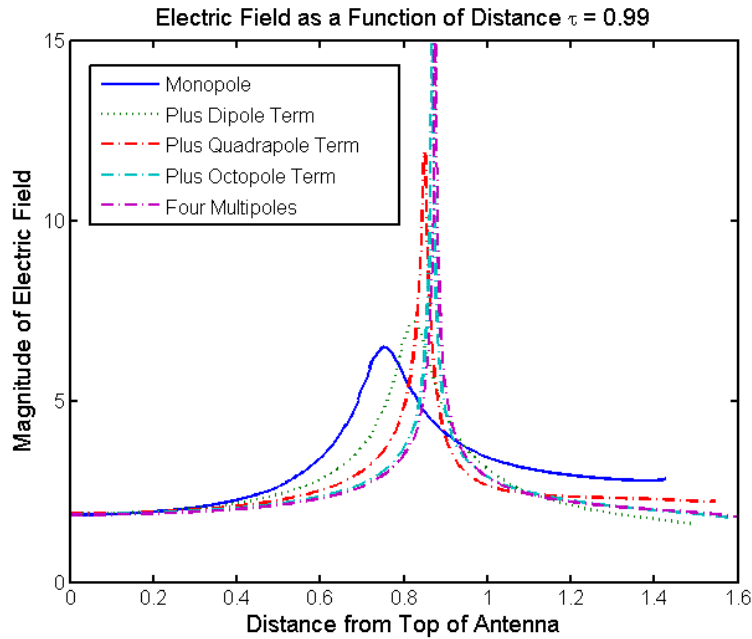


Figure 4. Electric field calculated as a function of distance from the antenna top.

## 5. SECTION CST MODEL OF OBLATE MONOPOLE ANTENNA

Computer Simulation Technology (CST) Microwave Studio T-solver was used to model the antenna; Figure 5 is a plot of the antenna surface with a 45° slice removed to highlight the edge. The tapered feed line in the antenna cannot be modeled with Microwave Studio. To simplify the CST model, the tapered feed line is replaced with a 1-cm-diameter hollow feed line. The hollow feed line was used to reduce the capacitance at the feed point. The small capacitance introduced by the feed line is estimated in this section.

An accurate model for the energy is critical for  $Q$  calculations; CST includes an energy-based adaptive meshing that increases the mesh resolution in areas of high-energy density. A sequence of adaptive meshing models was run to refine the starting mesh for the next model<sup>1</sup>. A 1-cm diameter, 4.3-ohm cylindrical edge port was used at the feed point. The current flows on the cylindrical edge port surface. A line source would have a much larger inductance.

The excitation frequency range was from 15 to 25 MHz; this reduces the energy reflected at the input to the antenna<sup>2</sup>. The hollow feed line was modeled independently to determine the required meshing. The CST calculation used the exact antenna geometry. The convergence in the solutions is evaluated by looking at the largest difference between previous and current reflection coefficient  $S_{11}$ . In the final run, this difference in  $S_{11}$  is 3.4e-4. This process was time consuming, but it eliminated the risk of using too fine a mesh and introducing numerical errors in the solution.

The antenna capacitance, inductance,  $Q$ , and effective height can be extracted from the CST impedance data with a MATLAB program. The data with a reflection coefficient,  $|\rho| \leq 0.9$ , is used in the analysis of the impedance. The MATLAB program calculated the least square best fit to Stuart's eigenmode impedance circuit model, Figure 6 and Table 1. The series  $C$  and  $L$  with a parallel resistance  $R_0$  represents the dipole eigenmode of the antenna. The fit to the reactance was very good but the radiation resistance has a large error. An additional octopole eigenmode can be modeled at low frequencies as a parallel capacitor  $C_{OP+}$ , where the subscript indicates octopole plus higher order eigenmodes (the inductors short the other circuit elements at low frequencies). This approximation is very accurate; the octopole eigenmode<sup>3</sup> is resonant at 242.22 MHz with only 3.17  $\Omega$  radiation resistance. The addition of the  $C_{OP+}^{OSA}$  eliminates the error in the numerical fit to the radiation resistance. The impact of  $C_{OP+}^{OSA}$  on the reactance is not significant. The superscript indicates the antenna type as an OSA (oblate spheroidal antenna). The circuit parameters are computed with an iteration process.

A two-step iteration process is used to minimize the error in the radiation resistance. The dipole eigenmode  $L^{OSA}$  and  $C^{OSA}$  values are a good approximation to the reactance; they are used as fixed inputs to a least square fit for  $R_0^{OSA}$  and  $C_{OP+}^{OSA}$ . The new  $R_0^{OSA}$  and  $C_{OP+}^{OSA}$  values are used as fixed inputs to a least square fit for improved  $L^{OSA}$  and  $C^{OSA}$  values. This iteration process was repeated until a self-consistent numerical solution was obtained. Figure 7 shows the CST impedance and the two

---

<sup>1</sup>Shrikrishna Hegde at Sonnent Software provided insight into energy adaptation and meshing.

<sup>2</sup>James Whillhite at Sonnent Software suggested matching the source resistance to the antenna resistance and using a narrow frequency range to maximize the energy delivered to the antenna.

<sup>3</sup>The antenna was excited by a short voltage pulse. After the initial excitation,  $V = 0$  at the feed point, the antenna is shorted to the ground.

eigenmode circuit approximation of the impedance. The difference is so small it is plotted in Figure 8. The errors introduced by the CST numerical computation and the eigenmode circuit model approximation are independent. The small difference between the two models indicates that both are accurate.

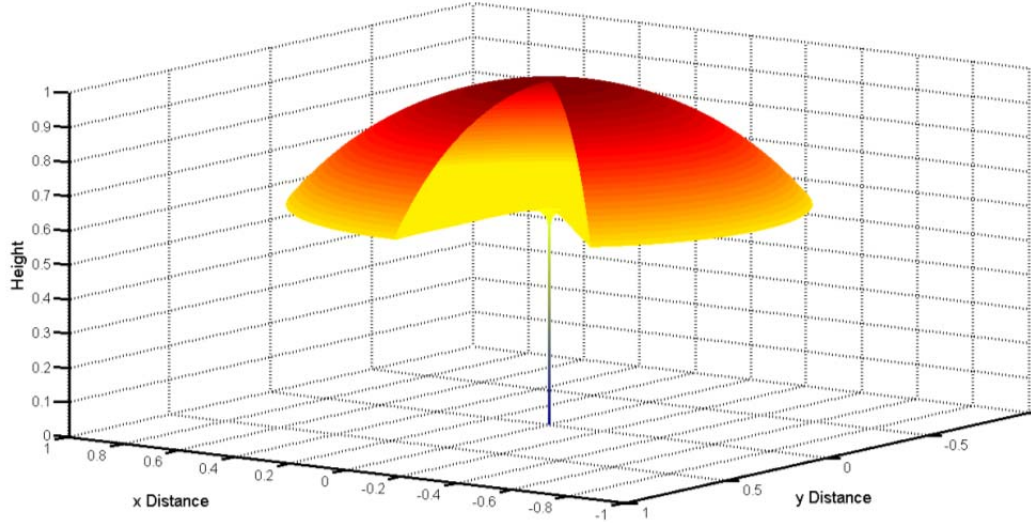


Figure 5. The three-dimensional OSA surface with a 45° slice removed.

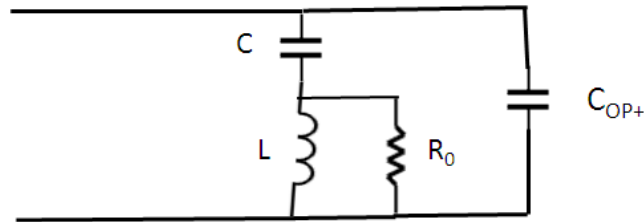


Figure 6. The equivalent circuit for the first and second eigenmode approximation.

The DC capacitance is

$$C_{DC\ CST}^{OSA} = C^{OSA} + C_{OP+}^{OSA} = 95.87. \quad (36)$$

The impact of the 1-cm-diameter hollow feed line can be estimated. The current on the feed line is almost constant; almost all of the charge flows onto the top load. A reasonable approximation for the charge distribution on the feed line is a triangular distribution. The net charge on the feed line is one-half the monopole charge distribution (constant charge distribution for electrically small monopole). The capacitance of the 0.587-m high monopole is 6.2 pF. The feed-line capacitance is about 3.1 pF. The quasi-static antenna design algorithm assumes 1% of the total charge is on the tapered OSA feed line; the capacitance is 0.9 pF ( $= 0.01 \cdot 90.364$  pF). This difference is  $C^{Stem} = 2.2$  pF.

The difference between the two calculations is about 3.3 pF or about 3.6%:

$$C_{DCQS}^{OSA} = C_{QS}^{OSA} + C^{Stem} = 92.56. \quad (37)$$

Table 1. Least square best fit to Stuart's eigenmode impedance circuit model.

Parameters	Eigenmode 1	Eigenmode 1 & 2	QSADA
$C_{DC}$		95.87	90.364 pF
$C^{OSA}$	90.15 pF	90.292385 pF	N/A
$L^{OSA}$	0.67295 uH	0.67164778 uH	N/A
$R_0^{OSA}$	1941.8 K $\Omega$	1942.7468 K $\Omega$	N/A
$f_0^{OSA}$	20.39706 MHz	20.458733 MHz	N/A
$h_{Eff}$	N/A	0.7063	0.7108
$C_{OP+}^{OSA}$	N/A	5.5793389 pF	N/A
Q-factor ratio at resonance	N/A	1.772	1.82
Q-factor ratio $a = \lambda / 40$	N/A		1.82

The impedance of the circuit is rewritten to give insight into the Figure 6 current flow. The quasi-static antenna design algorithm calculates the DC capacitance. The fraction of current flowing into the dipole eigenmode is  $\alpha^{OSA} = C^{OSA} / (C^{OSA} + C_{OP+}^{OSA}) = 0.94$ . In addition to current sharing, there is a circulating current flowing between the two eigenmodes. The  $\omega^2 \alpha^{OSA} L^{OSA} C_{OP+}^{OSA}$  increased the radiation resistance and inductance. The value  $\omega^2 \alpha^{OSA} L^{OSA} C_{OP+}^{OSA}$  is 0.058 near the resonance and 1 at the anti-resonance. The term  $\omega L^{OSA} / R_0^{OSA} = 0.044$  is also small near resonance. In the iteration process, changes in the value of  $R_0^{OSA}$  and  $C_{OP+}^{OSA}$  make an insignificant contribution to the reactance:

$$X_{Total}^{OSA} = \frac{1}{j\omega(C^{OSA} + C_{OP+}^{OSA})} + \left[ \frac{j\omega(\alpha^{OSA})^2 L^{OSA} (1 - \omega^2 \alpha L^{OSA} C_{OP+}^{OSA})}{\left[ (1 - \omega^2 \alpha^{OSA} L^{OSA} C_{OP+}^{OSA})^2 + (\omega L^{OSA} / R_0^{OSA})^2 \right]} \right],$$

$$R_{Total}^{OSA} = \left[ \frac{(\omega \alpha^{OSA} L^{OSA})^2 R_0^{OSA}}{\left[ (R_0^{OSA})^2 (1 - \omega^2 \alpha L^{OSA} C_{OP+}^{OSA})^2 + (\omega L^{OSA})^2 \right]} \right].$$

The term  $\omega^2 \alpha^{OSA} L^{OSA} C_{OP+}^{OSA}$  makes a larger contribution to the resistance near resonance, 12%. The resistance depends on the ratio  $(L^{OSA})^2 / R_0^{OSA}$  and  $C_{OP+}^{OSA}$ ; the values of  $L^{OSA}$  and  $C_{OP+}^{OSA}$  can be fixed without restricting the accuracy of the least squares fit to the resistance.

In the limit as  $\omega \rightarrow 0$ , the radiation resistance and Q reduces to

$$R_{Total}^{OSA} = \frac{(\omega \alpha^{OSA} L^{OSA})^2}{R_0^{OSA}},$$

where

$$Q_{Total}^{OSA} = \frac{1}{\omega(C^{OSA} + C_{OP+}^{OSA})R_{Total}^{OSA}}.$$

The above term can be simplified by introducing the  $Q_{Dipole EM}^{OSA}$ , where the subscript DipoleEM indicates the dipole eigenmode  $Q_{Dipole EM}^{OSA} = \frac{1}{\omega C^{OSA} R_{Dipole EM}^{OSA}}$ ,

where

$$R_{Dipole EM}^{OSA} = \frac{(\omega L^{OSA})^2}{R_0^{OSA}}.$$

The  $Q_{Dipole EM}^{OSA}$  of the dipole eigenmode is increased by  $1/\alpha^{OSA}$ , the same result cited by H. R. Stuart [18]:

$$Q_{Total}^{OSA} = Q_{Dipole EM}^{OSA} / \alpha^{OSA}.$$

The radiation resistance, Figure 9, has two components  $\omega^2$  and  $\omega^4$  terms,

$$R_{OSA} = b_1(\omega/\omega_r)^2 + b_2(\omega/\omega_r)^4,$$

where  $\omega_r$  is the angular resonant frequency,  $b_1 = 3.6465$  and  $b_2 = 0.4575$ . The effective height in Table 1 is calculated from the  $\omega^2$  term in the radiation resistance. The quasi-static antenna design algorithm is close to the value in Table 1; but, it does not include the current sharing factor  $\alpha^2$  in the radiation resistance. The current sharing factor increases the  $Q_{Dipole EM}^{OSA}$  by  $1/\alpha = 1.13$ . The octopole eigenmode increases the radiation resistance at higher frequencies.

The Q, shown in Figure 10 is numerically calculated from the fit data using the A. D. Yaghjian and S. R. Best [19] result:

$$Q = \frac{\omega}{2R} \sqrt{\left(\frac{dR}{d\omega}\right)^2 + \left(\frac{|X|}{\omega} + \frac{dX}{d\omega}\right)^2}. \quad (39)$$

Figure 11 shows the  $Q(ka)^3$  “Q-factor ratio” for the antenna that was calculated for an extended frequency range. The minimum Q-factor ratio is 1.77. The Q at resonance is 22.47.

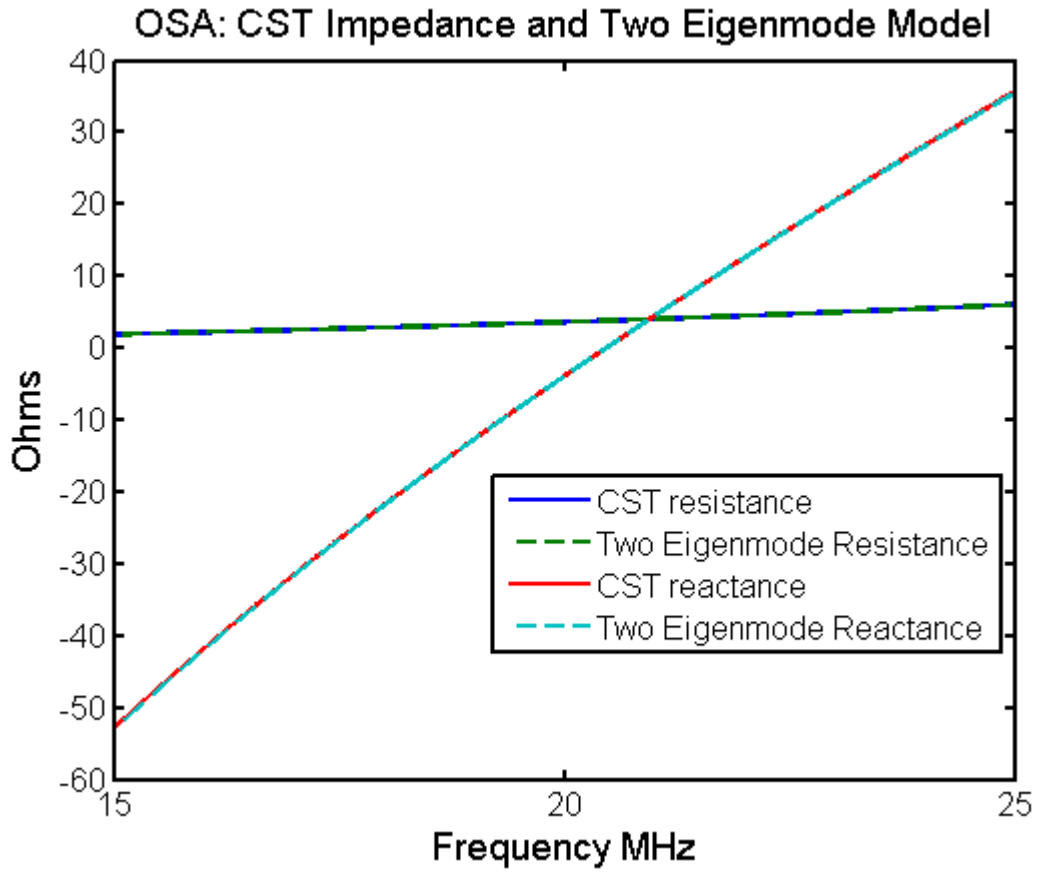


Figure 7. CST data and two-eigenmode equivalent circuit model.

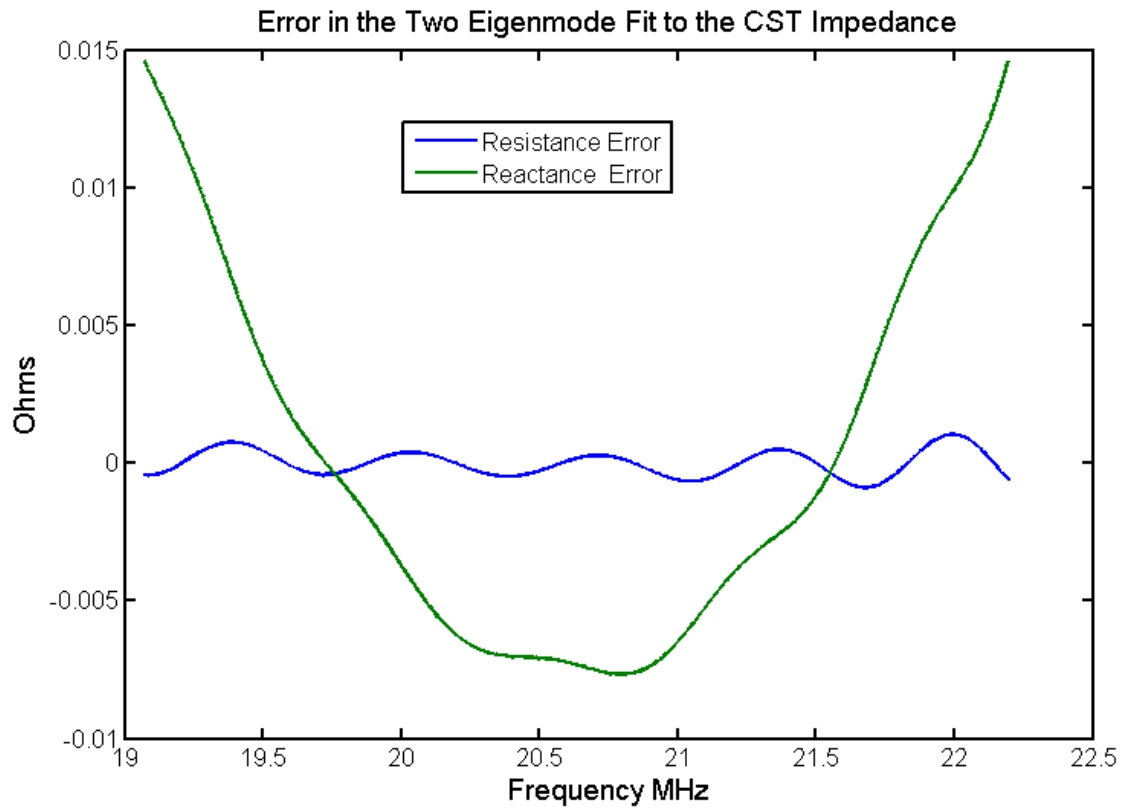


Figure 8. Difference between the CST data and the two-eigenmode model for  $|\rho| < 0.9$ .

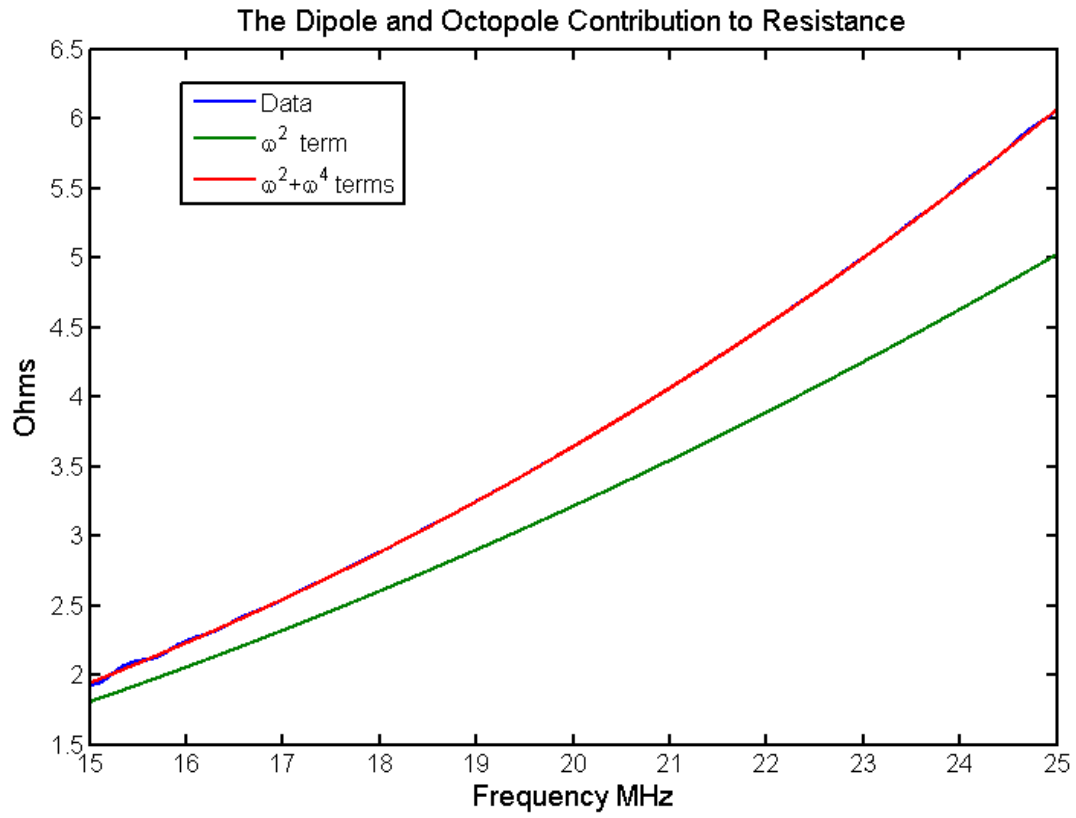


Figure 9. The  $\omega^2$  and  $\omega^4$  contribution to resistance.

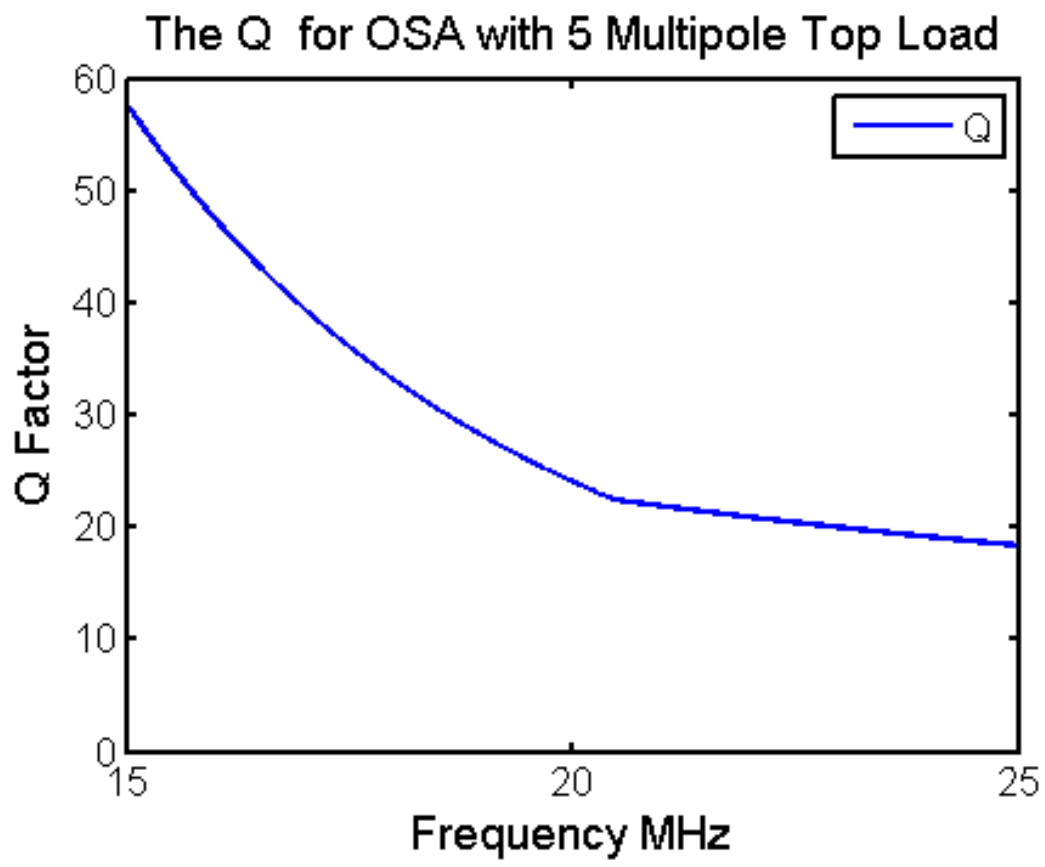


Figure 10. Q for the minimum Q OSA design.

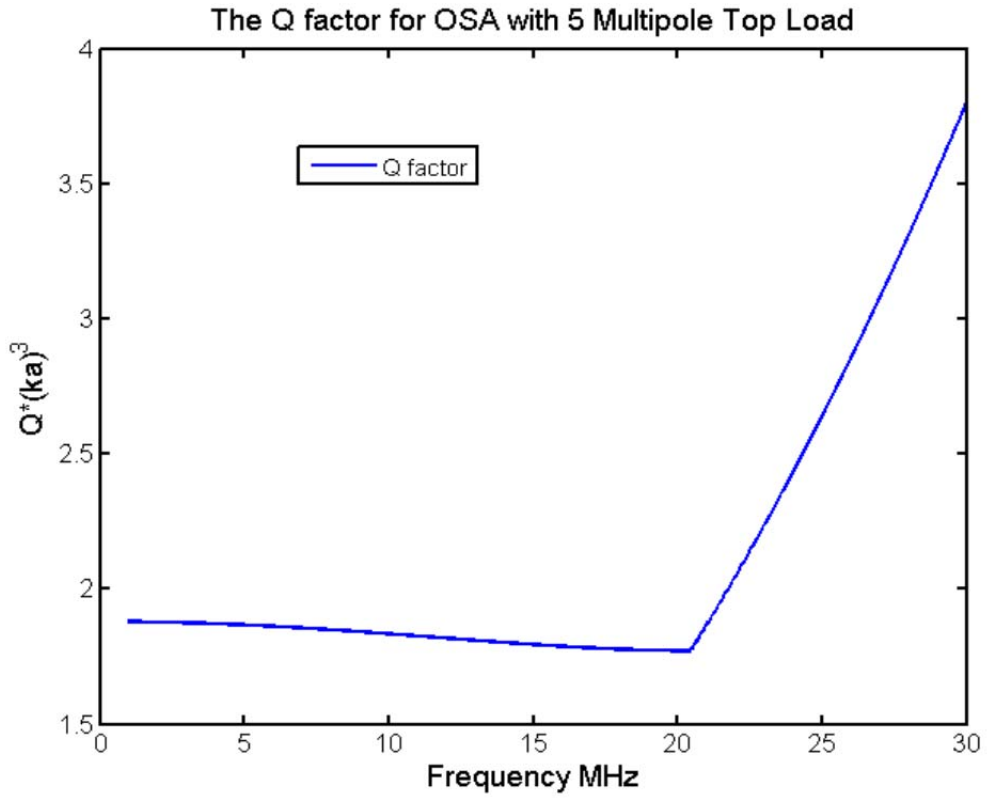


Figure 11. Q-factor ratio for the minimum Q OSA design.



## 6. CST MODEL OF A SPHERICAL-CAP MONOPOLE

The same method was used to model a spherical-cap monopole. The edge of the spherical-cap monopole requires a higher resolution CST model. If the edge thickness was set too small, CST will not accurately model the conductor and the electric field. An accurate model of the electric field is critical to the calculation of the Q. The shell thickness is 0.83 cm; the horizontal edge is 1 cm and the height of the edge is 0.556 m. A. R. Lopez [14] published a Q-factor ratio of  $Q(ka)^3 = 1.75$ , where  $a = 0.025\lambda$ .

The same MATLAB program was used to numerically fit the data to a two-eigenmode model, Table 2 and Figure 12. The superscript SP is for spherical-cap monopole. Figure 13 shows the magnitude of the resistance and reactance error is  $< 0.001\Omega$  and  $< 0.0022\Omega$ , respectively. The spherical-cap monopole has a larger surface area and a smaller charge density larger than the above antenna. The potential on the spherical-cap monopole will be smaller and the DC capacitance is 8% larger than the above antenna. The effective height is 5% smaller than the above antenna. The inductance of the spherical-cap monopole is 52% larger than the oblate spheroidal antenna. A thinner spherical shell will have less charge on the edge and a higher charge density on the sphere. The higher charge density increases the potential on the sphere, which decreases the capacitance. Moving the edge charge to a higher position increases the effective height. H. R. Stuart and A. D. Yaghjian [20] pointed out that a thicker shell has a higher Q-factor ratio. The feed-line analysis is the same as above. A 1-m monopole has 9.54-pF capacitance. The feed line would have a capacitance around 5 pF. The CST model is reasonably accurate. The higher inductance reduces the resonance to 15.88 MHz. The Q at resonance is 46.1, much higher than the oblate spheroidal antenna.

The radiation resistance, shown in Figure 14, has two components,  $\omega^2$  and  $\omega^4$ :

$$R_{SP} = s_1(\omega/\omega_r)^2 + s_2(\omega/\omega_r)^4, \quad (40)$$

where  $\omega_r$  is the angular resonant frequency,  $s_1 = 1.9427$  and  $s_2 = 0.2768$ . The Q is plotted in Figure 15 and the Q-factor ratio is plotted in Figure 16.

Table 2. Spherical-cap monopole impedance fit to a two-eigenmode model.

Parameters	Eigenmode 1	Eigenmode 1 & 2
$C^{SP}$	97.854775 pF	97.925944 pF
$L^{SP}$	1.0263675 $\mu$ H	1.0254508 $\mu$ H
$R_0^{SP}$	4719.2571 $\Omega$	4718.4470 $\Omega$
$f_0^{SP}$	15.90688 MHz	15.88625 MHz
$h_{Eff}$	N/A	0.6619
$C_{OP+}^{SP}$	N/A	6.1185130 pF
<i>Q-Factor</i>	N/A	1.70

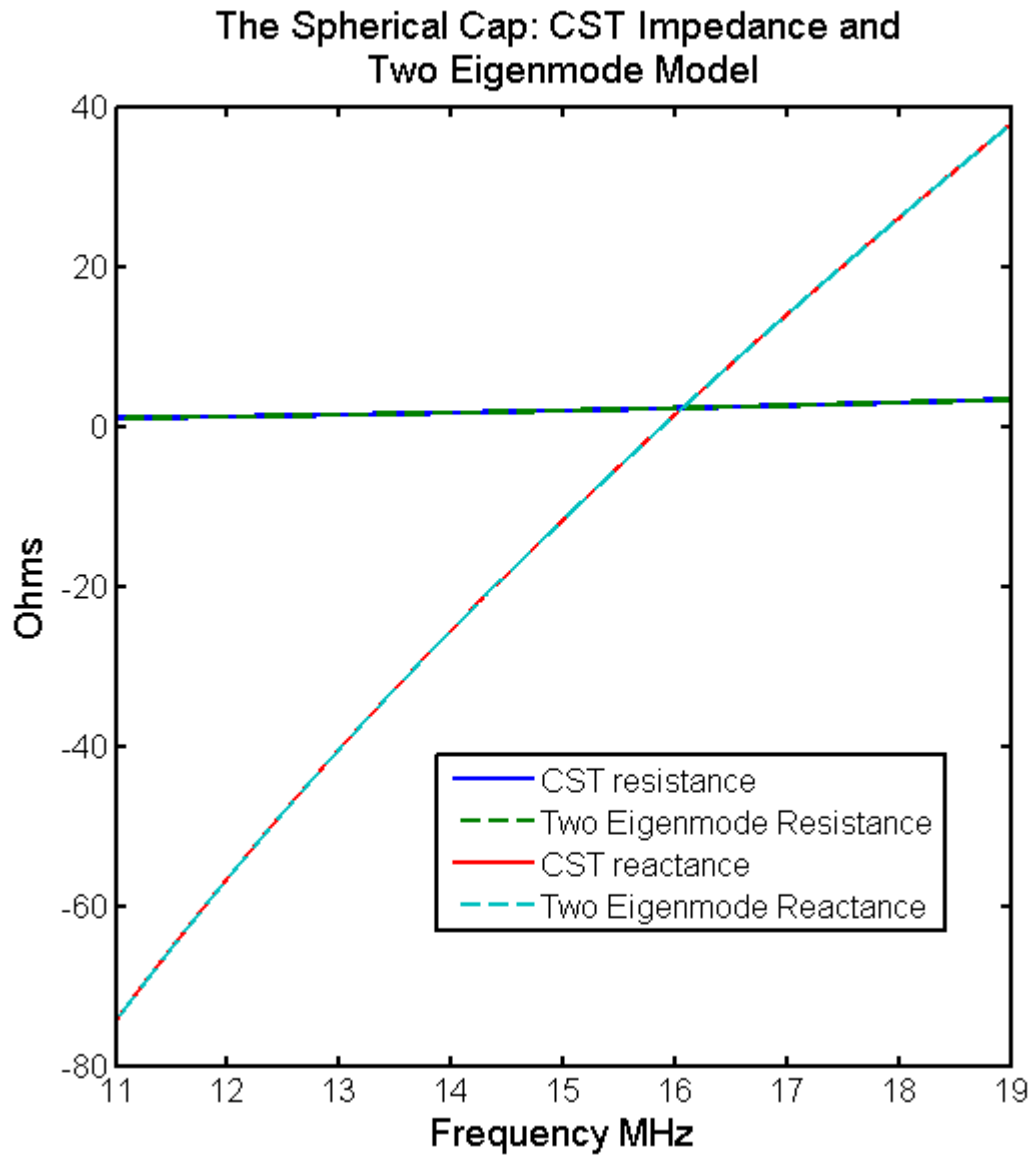


Figure 12. CST impedance and two-eigenmode model.

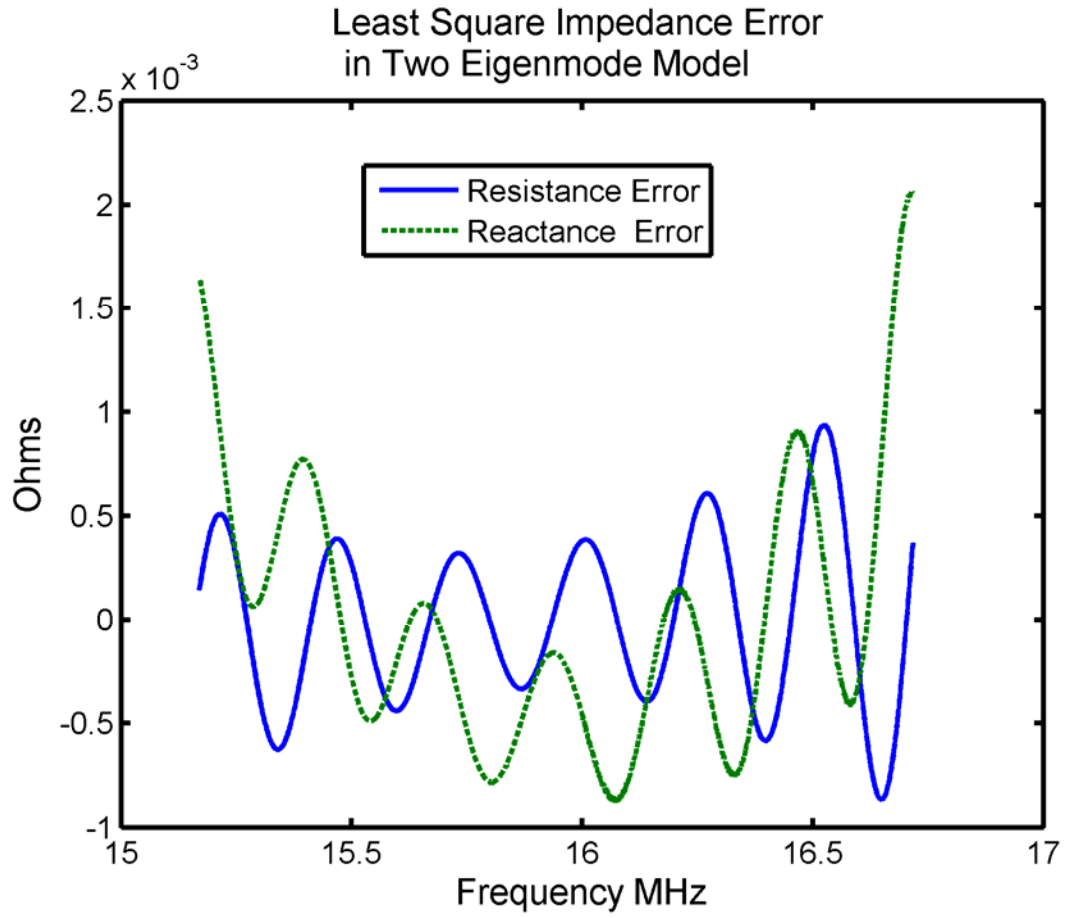


Figure 13: Difference between the CST data and the two-eigenmode model.

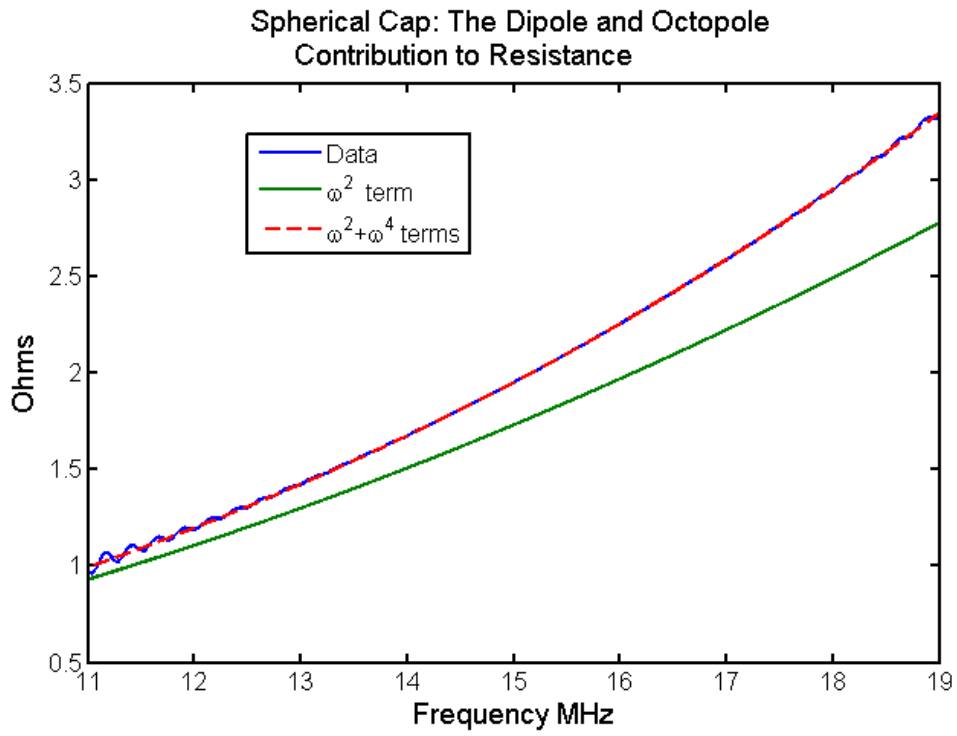


Figure 14. The  $\omega^2$  and  $\omega^4$  components of resistance.

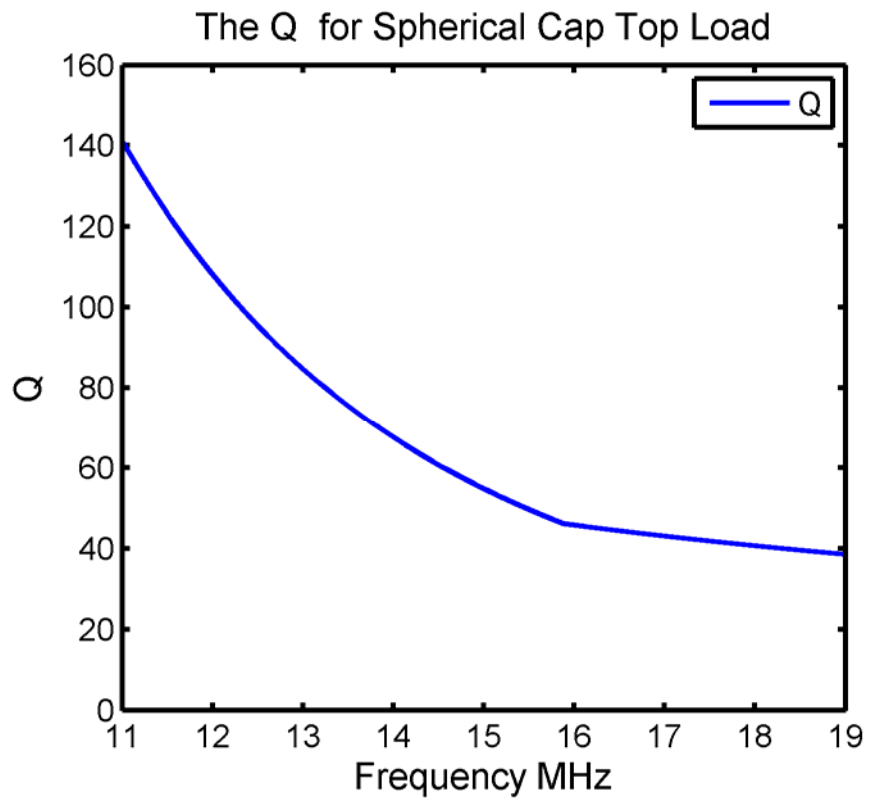


Figure 15. Q for spherical-cap monopole.

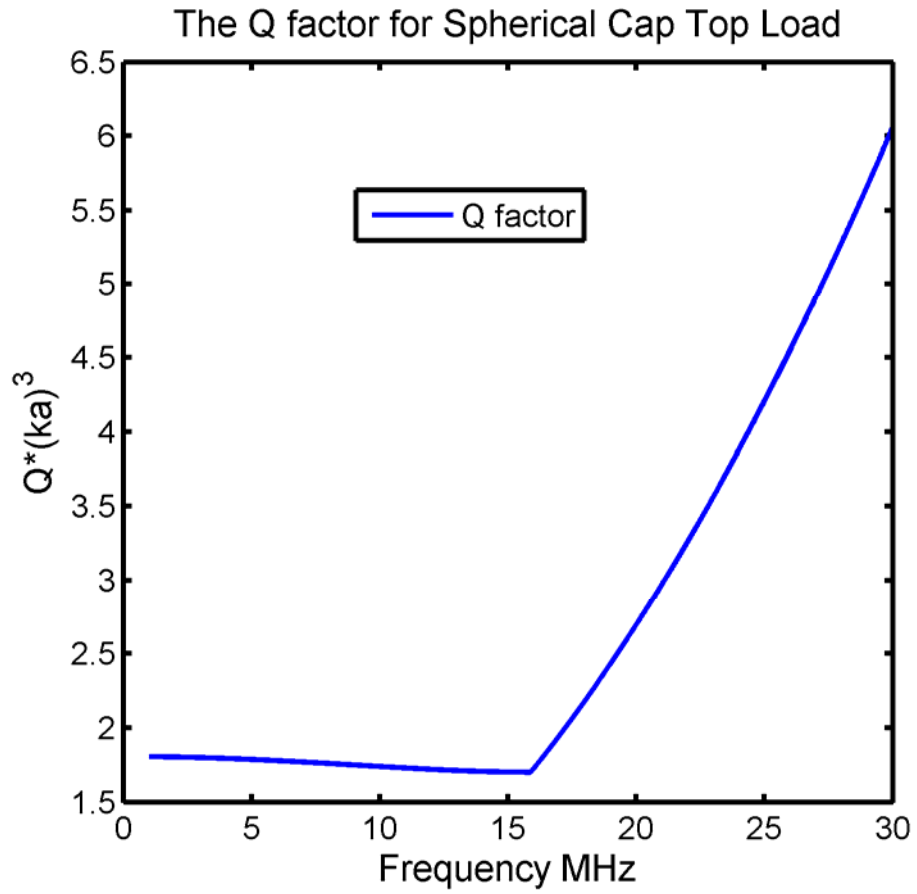


Figure 16. Q-factor ratio for spherical-cap monopole.

## 7. CONCLUSION

The quasi-static antenna design algorithm modeled a thick-disk cap as a sum of multipole moments. The algorithm appears to converge in Q and shape. In the case of a spherical enclosure, the Q is only slightly larger than the minimum Q spherical-cap monopole. Above the resonant frequency of the oblate spheroidal antenna, the Q is one-half of the spherical-cap monopole. This is caused by the reduced inductance of the feed line. This increases the resonant frequency and greatly reduces the Q.

This algorithm only included solutions with the (charge distribution) disk enclosed inside the antenna surface. The allowed solutions are limited to the thick-disk-cap dipole. A thick-spherical-cap monopole could be thick at the center and taper to a thin edge. The thick center could reduce the stored energy under the spherical cap. The dipole moment and radiation resistance would be reduced. The thick-spherical cap could reduce Q-factor ratio.

The electromagnetic properties of an antenna can be described as a linear combination of eigenmodes. The quasi-static antenna design algorithm is a method for calculating the radiation resistance of the dipole eigenmode (the  $\omega^2$  term) and the DC capacitance of the antenna. The three-element circuit model of the dipole eigenmode impedance does not accurately explain the impedance and Q. An accurate model for the impedance requires a contribution from the octopole and higher eigenmodes. The octopole and higher eigenmode can be approximated with a parallel capacitor. The interaction of the dipole and octopole eigenmode introduces the  $\omega^4$  term required in the radiation resistance.

The quasi-static antenna design algorithm ignores the octopole and higher order eigenmodes of the antenna. The current sharing between the dipole eigenmode and higher eigenmodes is also ignored. This introduces a small error in the Q and dipole eigenmode radiation resistance. The circulating current in the circuit model increases both the effective radiation resistance and the effective inductance.

The quasi-static antenna design algorithm is an excellent approximation of electrically small antennas. In most cases, the error caused by the current sharing factor ratio should be insignificant.



## 8. REFERENCES

1. L. J. Chu. 1948. "Physical Limitations of Omnidirectional Antennas," *Journal of Applied Physics*, vol. 19, no. 12 (December), pp. 1163–1175.
2. H. L. Thal. 2006. "New Radiation Q Limits for Spherical Wire Antennas," *IEEE Transactions Antennas and Propagation*, vol. 54, no. 10 (October), pp. 2757–2763.
3. S. R. Best. 2004. "The Radiation Properties of Electrical Small Folder Spherical Helix Antennas," *IEEE Transactions Antennas and Propagation*, vol. 52 (April), pp. 953–959.
4. M. Gustafsson, C. Sohl, and G. Kristensson. 2009. "Illustrations of New Physical Bounds on Linearly Polarized Antennas," *IEEE Transactions on Antennas and Propagation*, vol. AP-57, no. 5 (May), pp. 1319–1327.
5. A. D. Yaghjian and H. R. Stuart. 2010. "Lower Bounds on the Q of Electrically Small Dipole Antennas," *IEEE Transactions on Antennas and Propagation*, vol. 58, no. 10 (October).
6. T. O. Jones III. 2012. Quasi-Static Design Approach for Minimizing the Quality Factor '  $Q$  ' for Electrical Small Antennas, U.S. Patent 8,121,821 B1 (February 21).
7. T. O. Jones III. 2011. "A Quasi-Static Antenna Design Approach for Minimum-Q Antennas," *IEEE Antennas and Propagation Magazine*, vol. 53, no. 3 (June), pp. 84-94.
8. T. O. Jones III. 2013. Dipole Moment Term for an Electrically Small Antenna, U.S. Patent 8368156 B1 (February 5).
9. S. A. Schelkunoff and H. T. Friis. 1952. *Antennas, Theory and Practice*, p. 318, Figure 10.9, John Wiley & Sons, Inc., New York, NY.
10. N. C. De, T. K. Ghosh, D. R. Poddar, and S. K. Chowdhury. 1995. "Design and Experimental Investigation of the Asymptotic Conical Dipole Antenna," *IEEE Transactions on Electromagnetic Compatibility*, vol. 37, no. 2 (May), pp. 282–285.
11. T. Simpson. 2006. "The Scheikunaff-Friis Dipole: the Simplest Antenna of All," *IEEE Antennas and Propagation Magazine*, vol. 48, no. 4 (August), pp. 48–53.
12. H. D. Foltz, J. S. McLean, and L. Bodner. 2002. "Closed-form Lumped Element Model for Folded, Disk Loaded Monopoles." *Proceedings of IEEE Antennas and Propagation Society International Symposium* (pp. 576–579). 16-21 June, San Antonio, TX.
13. H. R. Stuart. 2009. "Eigenmode Analysis of a Two Element Segmented Capped Monopole Antenna," *IEEE Transactions on Antennas and Propagation*, vol. 57, no. 10 (October), pp. 2980–2888.
14. A. R. Lopez. 2006. "Fundamental Limits of Small Antennas: Validation of Wheeler's Formula," *IEEE Antenna and Propagation Magazine*, vol. 48, no. 4 (August), pp. 28–35.
15. The author derived this result from [16]; he is not first to calculate this result.
16. I. S. Gradshteyn and I. M. Ryzhik. 1980. *Table of Integrals, Series, and Products*, Corrected and Enlarged Edition, Fourth Edition. Academic Press, New York, NY.
17. G. Arfken. 1970. *Mathematical Methods for Physicists*, Second Edition. Academic Press, New York, NY.

18. H. R. Stuart. 2012. "Understanding the Bandwidth Limitations of Small Antennas: Wheeler, Chu and Today," *Antennas and Propagation Society International Symposium (APSURSI)* (pp. 1–2). 8–14 July, Chicago, IL. Institute of Electrical and Electronics Engineers (IEEE).
19. A. D. Yaghjian and S. R. Best. 2005. "Impedance, Bandwidth and  $Q$  of Antenna," *IEEE Transactions on Antennas and Propagation*, vol. 53, no. 4 (April), pp. 1298–1324.
20. H. R. Stuart and A. D. Yaghjian. 2010. "Approaching the Lower Bounds on  $Q$  for Electrically Small Electric-Dipole Antennas Using High Permeability Shells," *IEEE Transactions on Antennas and Propagation*, vol. 58, no. 12 (December), pp. 3865–3872.

**REPORT DOCUMENTATION PAGE**

*Form Approved  
OMB No. 0704-01-0188*

The public reporting burden for this collection of information is estimated to average 1 hour per response, including the time for reviewing instructions, searching existing data sources, gathering and maintaining the data needed, and completing and reviewing the collection of information. Send comments regarding this burden estimate or any other aspect of this collection of information, including suggestions for reducing the burden to Department of Defense, Washington Headquarters Services Directorate for Information Operations and Reports (0704-0188), 1215 Jefferson Davis Highway, Suite 1204, Arlington VA 22202-4302. Respondents should be aware that notwithstanding any other provision of law, no person shall be subject to any penalty for failing to comply with a collection of information if it does not display a currently valid OMB control number.

**PLEASE DO NOT RETURN YOUR FORM TO THE ABOVE ADDRESS.**

<b>1. REPORT DATE (DD-MM-YYYY)</b> April 2013		<b>2. REPORT TYPE</b> Final		<b>3. DATES COVERED (From - To)</b>										
<b>4. TITLE AND SUBTITLE</b>  Convergence of the Quasi-static Antenna Design Algorithm				<b>5a. CONTRACT NUMBER</b>										
				<b>5b. GRANT NUMBER</b>										
				<b>5c. PROGRAM ELEMENT NUMBER</b>										
<b>6. AUTHORS</b>  T. O. Jones III				<b>5d. PROJECT NUMBER</b>										
				<b>5e. TASK NUMBER</b>										
				<b>5f. WORK UNIT NUMBER</b>										
<b>7. PERFORMING ORGANIZATION NAME(S) AND ADDRESS(ES)</b>  SSC Pacific 5622 Hull Street San Diego, CA 92152-5001				<b>8. PERFORMING ORGANIZATION REPORT NUMBER</b>  TR 2016 Rev. 1										
<b>9. SPONSORING/MONITORING AGENCY NAME(S) AND ADDRESS(ES)</b>  None				<b>10. SPONSOR/MONITOR'S ACRONYM(S)</b>										
				<b>11. SPONSOR/MONITOR'S REPORT NUMBER(S)</b>										
<b>12. DISTRIBUTION/AVAILABILITY STATEMENT</b>  Approved for public release.														
<b>13. SUPPLEMENTARY NOTES</b>  This is work of the United States Government and therefore is not copyrighted. This work may be copied and disseminated without restriction.														
<b>14. ABSTRACT</b>  The quasi-static antenna-design algorithm uses multipole basis function to model the general thick top load. A sequence of solutions converge in shape and Q. The absolute minimum Q-factor, 1,825, is obtained for a thick disk top load enclosed by a sphere. This is significantly smaller than the thin disk top load Q-factor 2.349 and previously derived thick-disk Q-factor 2.078. An analytic potential is derived for each multipole basis function. The capacitance and effective height is calculated from the potentials on the enclosing sphere. The impedance is computed with Computer Simulation Technology (CST) Microwave Studio. The impedance data is numerically fit to a dipole eigenmode equivalent circuit. The radiation resistance does not fit the expected $\omega^2$ frequency dependence (effective height).  The error is an $\omega^4$ term that is explained by a capacitor approximated for the octupole eigenmode equivalent circuit. The quasi-static antenna design algorithm predicts the DC capacitance and the dipole eigenmode effective height. The octupole eigenmode increases the radiation resistance. The Q-factor, 1.77, is lower than expected. These results are compared to the spherical cap top load. The existence of an $\omega^4$ limits the accuracy of the theoretical limits in the Q values for antennas.														
<b>15. SUBJECT TERMS</b> <table style="width:100%; border:none;"> <tr> <td style="width:33%;">oblate spheroidal antenna</td> <td style="width:33%;">Q-factor</td> <td style="width:33%;">multipole basis function</td> </tr> <tr> <td>radiation resistance</td> <td>quasi-static antenna</td> <td>equivalent circuit model</td> </tr> <tr> <td>top load</td> <td>dipole eigenmode</td> <td>two-eigenmode circuit model</td> </tr> </table>						oblate spheroidal antenna	Q-factor	multipole basis function	radiation resistance	quasi-static antenna	equivalent circuit model	top load	dipole eigenmode	two-eigenmode circuit model
oblate spheroidal antenna	Q-factor	multipole basis function												
radiation resistance	quasi-static antenna	equivalent circuit model												
top load	dipole eigenmode	two-eigenmode circuit model												
<b>16. SECURITY CLASSIFICATION OF:</b>			<b>17. LIMITATION OF ABSTRACT</b>	<b>18. NUMBER OF PAGES</b>	<b>19a. NAME OF RESPONSIBLE PERSON</b>									
a. REPORT	b. ABSTRACT	c. THIS PAGE			T. O. Jones III									
U	U	U	U	46	<b>19b. TELEPHONE NUMBER (Include area code)</b> (619) 553-7082									



## INITIAL DISTRIBUTION

84300	Library	(2)
85300	Archive/Stock	(1)
52260	T. O. Jones III	(1)

Defense Technical Information Center		
Fort Belvoir, VA 22060-6218		(1)





Approved for public release.



SSC Pacific  
San Diego, CA 92152-5001